Atmos. Chem. Phys. Discuss., 12, 2355–2394, 2012
www.atmos-chem-phys-discuss.net/12/2355/2012/
doi:10.5194/acpd-12-2355-2012

Atmospheric Chemistry and Physics Discussions

Aerosol observations and growth rates in the tropical tropopause layer

D. A. Waddicor[1], G. Vaughan[1], T. W. Choularton[1], K. N. Bower[1], H. Coe[1], M. Gallagher[1], P. I. Williams[1], M. Flynn[1], A. Volz-Thomas[2], W. Pätz[2], P. Isaac[3], J. Hacker[3], F. Arnold[4], H. Schlager[5], and J. A. Whiteway[6]

[1]School of Earth, Atmospheric and Environmental Sciences, The University of Manchester, UK
[2]Forschungszentrum Jülich, Germany
[3]Flinders University, Adelaide, Australia
[4]Max-Planck-Institute for Nuclear Physics, Heidelberg, Germany
[5]Deutsches Zentrum für Luft- und Raumfahrt, Oberpfaffenhofen, Germany
[6]Centre for Research in Earth and Space Sciences, York University, Toronto, Canada

Received: 6 January 2012 – Accepted: 11 January 2012 – Published: 25 January 2012

Correspondence to: G. Vaughan (geraint.vaughan@manchester.ac.uk)

Published by Copernicus Publications on behalf of the European Geosciences Union.

Abstract

We present a case study of Aitken and accumulation mode aerosol observed downwind of the anvils of deep tropical thunderstorms. The measurements were made by condensation nuclei counters flown on the Egrett high-altitude aircraft from Darwin during the ACTIVE campaign, in monsoon conditions producing widespread convection over land and ocean. Maximum measured concentrations of aerosol in the size range 10–100 nm were 25 000 cm^{-3} STP. By calculating back-trajectories from the observations, and projecting on to infrared satellite images, the time since the air exited cloud was estimated. In this way a time scale of ∼3–4 h was derived for the 10–100 nm aerosol concentration to reach its peak. We examine the hypothesis that the growth in aerosol concentrations can be explained by production of sulphuric acid from SO_2 followed by particle nucleation and coagulation. Estimates of the sulphuric acid production rate show that the observations are only consistent with this hypothesis if the particles coagulate to sizes > 10 nm much more quickly than is suggested by current theory. Alternatively, other condensible gases (possibly organic) drive the growth of aerosol particles in the TTL.

1 Introduction

1.1 Aerosol population in the Tropical Tropopause Layer

This paper presents a case study of aerosol measurements in the Tropical Tropopause Layer (TTL) and estimates the time scale for the growth of new aerosol to Aitken mode sizes (≥ 10 nm). The TTL is the region from approximately 14–18 km altitude (Füglistaler et al., 2009), above the main convective outflow and below the stratosphere. The importance of understanding aerosol processes in this region arises from the role of aerosol in the formation of cirrus cloud (Seifert et al., 2004a; Gallagher et al., 2005; Wang, 2005a,b; Choularton et al., 2008) and concomitant effect on the Earth's radiation budget.

A wide range of aerosol concentration has been observed in the upper troposphere during field campaigns. Brock et al. (1995) reported maximum values of $\sim 8000\,cm^{-3}$ (STP) for particles greater than 8 nm in diameter around 2 km below the tropical tropopause while Schröder and Ström (1997) reported a median concentration of $1400\,cm^{-3}$ (STP, diameter > 18 nm) above 4 km over Europe, but with maxima as high as $20\,000\,cm^{-3}$ (STP). The CARIBIC programme (Heintzenberg et al., 2003; Hermann et al., 2003; Brenninkmeijer et al., 2007) placed air sampling equipment on commercial flights between Germany and Namibia/South Africa, crossing the convectively active equatorial tropics over land that had undergone considerable biomass burning. Heintzenberg et al. (2003) found very high concentrations (10 000–$30\,000\,cm^{-3}$ STP) of particles with diameters between 4 and 12 nm, and a median concentration of $9000\,cm^{-3}$ (STP) for those with diameters between 12 and 18 nm. Such events coincided with deep convection, particularly in the tropics and subtropics, a result confirmed by later CARIBIC flights (Hermann et al., 2008). Similarly, Twohy et al. (2002) found extremely large concentrations of aerosol downwind of the outflow from a mesoscale convective storm (MCS): $45\,000\,cm^{-3}$ (STP) for particles ≥ 25 nm, spread over a 600 km region. These high particle concentrations were correlated with various trace gases, such as methane, carbon monoxide and nitrogen oxides, which were measured with similar concentrations inside the convective cloud region, indicating the air had passed through the storm before flowing downwind. No correlation was found with cloud particles, suggesting that the aerosol production was independent of cloud formation/evaporation. According to Clement et al. (2002), an estimated 5 h elapsed between air exiting cloud and the observations of $45\,000\,particles\,cm^{-3}$.

A comprehensive summary of ultrafine aerosol measurements in the TTL was provided by Borrmann et al. (2010) and Weigel et al. (2011), based mainly on aircraft campaigns with the M55 Geophysica and DLR Falcon. A key result of these papers is the maximum in particle concentration around 350 K potential temperature, near the main outflow region for deep tropical convection.

These studies show that convection can lead to high concentrations of TTL aerosol particles, but the mechanism causing such events is not understood. The intense precipitation experienced in convective systems removes most of the pre-existing aerosol in the lower reaches of the storms. The anvil outflow eventually evaporates, leaving a cloud-free environment with low particle surface area; such clean, low temperature conditions favour aerosol nucleation (Perry and Hobbs, 1994; Ström et al., 1999; Andreae et al., 2001; Clement et al., 2002; Kulmala et al., 2006). Despite the fact that the chemical identities and concentrations of condensing and nucleating gases are not known with certainty, a key candidate is gas-phase sulphuric acid, which was originally detected in the tropopause region by Möhler and Arnold (1992), using an aircraft-based mass spectrometer. This gas is formed by OH-induced SO_2 conversion to SO_3, followed by the reaction of SO_3 with water vapour. Modelling studies suggest that most of the SO_2 entering a thunderstorm is able to reach the anvil (see, e.g., Fiedler et al., 2009). Inside the anvil cloud, H_2SO_4 is readily adsorbed onto ice particles, but immediately downwind of the anvil the particle surface area is vastly reduced so new aerosols are formed (Twohy et al., 2002). Recently Fiedler et al. (2011) reported on SO_2 measurements made in biomass burning plumes above tropical Africa, also using a mass spectrometer. In an aged (about 10 days) biomass burning plume lifted to about 11 km by wet convection they measured SO_2 mixing ratios up to 100 pptv. From this number an initial SO_2 concentration in the plume of order 500 pptv may be estimated, taking into account plume dilution and reaction of SO_2 with OH. By contrast, in an aged (also about 10 days) biomass burning plume lifted by dry convection to about 4 km altitude they observed markedly increased SO_2 (up to 1400 pptv) and elevated particle number concentrations. Long-range transport from major anthropogenic SO_2 source regions may also lead to markedly increased upper troposphere SO_2 (Fiedler et al., 2009). Therefore, substantial spatial and temporal variability of SO_2 entering convective systems may be expected.

Nucleation in the TTL is believed to follow a binary (water and sulphuric acid) nucleation pathway, with the possible assistance of ions (Yu and Turco, 2001; Laakso

et al., 2002, 2003, 2007) and/or organic compounds (Kulmala et al., 2006; Sihto et al., 2006). According to this hypothesis, sulphuric acid condenses to molecular clusters that are sufficiently energetically stable (reach a critical size) for continuous vapour deposition to occur; this growth will continue into detectable aerosol size ranges (~ 3 nm), provided there is an adequate supply of condensable material (Clement et al., 2006; Boy et al., 2008). After the total surface area density of newly formed particles has increased sufficiently, condensation occurs preferably on these particles and nucleation ceases.

1.2 Modelling of aerosol nucleation and growth

Clement et al. (2006) presented a modelling study of the rate of aerosol nucleation and its controlling factors. The model was set up to simulate the evolution of acid production via SO_2 and OH radicals throughout the day. The OH concentration maximum occurs at mid-day, when the photodissociation of ozone is greatest, and the production of acid was halted at night (after 7 h in their simulation). This was parameterized as a maximum H_2SO_4 production rate of 10^5 molecules cm^{-3} s^{-1} from an estimated SO_2 concentration of 1 ppbv. Their analysis showed that after 21 min a nucleation mode (~ 3 nm) burst appeared. After 2 h, a "shoulder" appeared in the size distribution as condensational growth continued on the nucleated particles and coagulation occurred (see Fig. 1). The nucleation peak remained large as long as acid production remained high. These simulations showed that the maximum concentration of aerosol with diameters above 20 nm (see Fig. 1) was typically 10^3–10^4 cm^{-3}; the total aerosol concentration (≥ 3 nm) was between 10^4 and 10^6 cm^{-3}. The final number of aerosol produced was found to be independent of the initial number of nucleated particles and was related more to the acid production rate. This production only occurred in daylight; beyond this, nucleation mode aerosol coagulated into the larger size ranges and the remaining acid condensed onto any aerosol present. Clement et al. (2006) suggested that nucleation events require the background aerosol concentration to be below a threshold value, depending on the SO_2 and acid source rates.

2 Experimental details

2.1 The ACTIVE campaign

This study uses aerosol data from the "Aerosol and Chemical Transport in tropIcal conVEction" (ACTIVE) campaign conducted from Darwin, in the Northern Territory of Australia (Fig. 2) in the wet season of 2005/2006. This campaign took advantage of the regularity of deep convective storms in this region to investigate the composition of air uplifted by convection, and was primarily based around two research aircraft platforms: the Airborne Research and Survey (ARSF) Dornier (Allen et al., 2008), for low-level measurements and the Airborne Research Australia (ARA) Egrett, for high altitude outflow sampling and cirrus analysis. Details of the payloads and of the overall campaign are given by Vaughan et al. (2008). This study also uses data from the Falcon aircraft acquired during the concurrent SCOUT-O3 campaign in Darwin (Vaughan et al., 2008). The ACTIVE campaign covered two month-long periods: the first (November–December 2005) experienced pre-monsoon conditions, in an environment polluted by recent biomass burning; while the second (January–February 2006) experienced both an active monsoon and monsoon break conditions (May et al., 2008). The monsoon wind was maritime in origin (north westerlies) and hence the environment was far cleaner, with fewer fine particulates, in the second period. A summary of the low-level aerosol and gas measurements during ACTIVE is given by Allen et al. (2008).

This paper will present a case study of a flight of the Egrett aircraft from the monsoon phase of the ACTIVE campaign. It took place on the 23 January 2006, during the dissipation of a large monsoon system that spawned the previous day over the Central Northern Territories and then moved to the coast (a large mesoscale convective system developed later in the day, as this storm decayed).

2.2 Aircraft and payload

The aerosol measurements reported here are based on TSI 3010 condensation particle counters (CPCs), two of which were flown on the Egrett and one on the Dornier.

The latter, and one of the Egrett CPCs, operated with a temperature difference between saturator and condenser of 17° and a flow rate of 1 l min^{-1}; this gives a nominal 50 % detection efficiency for particles with diameter d = 10 nm. More precisely, the detection efficiency curve $E(d)$, may be approximated by the function:

$$E(d) = 1 - a(1 + \exp((d - D_1)/D_2))^{-1}, d \geq D_0, \quad (1)$$
$$E(d) = 0, d < D_0$$

where $D_0 = D_2 \ln(a-1) + D_1$ with a = 1.15, D_1 = 11.3 nm and D_2 = 2.1 nm (Wiedensohler et al., 1997). This formula gives a 50 % detection efficiency at 11.9 nm diameter.

A correction formula derived by Seifert et al. (2004b) from measurements in pressure chambers was applied to the Egrett data to allow for reduced counting efficiency at low pressure:

$$\text{count efficiency}, \eta = 1 - \alpha \exp(-\beta p / p_0) \quad (2)$$

where α = 1.627, β = 16.215, p_0 = 1013 hPa, and p (hPa) is the ambient pressure. At 200 mb, η=0.94.

The second CPC used on the Egrett was fitted with three diffusion disks to increase the lower size cut-off by removing smaller aerosol from the flow. As shown by Feldpausch et al. (2006) this cut-off is in fact very gradual, and the instrument remained sensitive to particles down to 20–30 nm in diameter, despite the nominal cut-off (50 % point) in detection efficiency of 100 nm at 200 mb.

The Egrett aerosol inlet was mounted on the port wing of the aircraft, protruding forward into the flow (Fig. 3) ahead of the propeller wash. It was built to a similar design to that used in the CARIBIC experiment (Hermann et al., 2001), to provide isokinetic sampling (the flow speed inside the inlet tip matches the undisturbed flow past the inlet housing). For the size range of particles considered in this study (10–1000 nm), Hermann et al. (2001) calculated that an inlet of this type would have a 90 % transmission efficiency; larger particles will be lost due to impaction, smaller ones through diffusion to the wall.

There was, however, a further seven metres of stainless steel piping leading from the inlet to the fuselage of the aircraft where the CPCs were mounted, introducing potential loss of Aitken mode particles by diffusion to the walls. A transmission function for aerosol as a function of size was derived for this pipe using the model of Gormley and Kennedy (1949). This gave a 56 % transmission for a diameter of 10 nm, 80 % for 20 nm and > 90 % beyond 40 nm – a function comparable to the efficiency curve of the CPC. A check on the validity of this prediction for accumulation mode particles was obtained by an intercomparison flight between the Egrett and the identical CPC on the Dornier, where the inlet length was only 2 m (for details of the Dornier aerosol inlet, see Allen et al., 2008). The two aircraft were flown "wing-tip-to-wing-tip", so that matching instrumentation from each aircraft should provide statistically identical results. The intercomparison flight took place in the boundary layer, where the aerosol was mainly in the accumulation mode. The Egrett instrument measured a slightly higher concentration than the Dornier's (Fig. 4), but within the manufacturer's quoted uncertainty for particle concentration. These results confirm that the pipework did not affect the transmission of the boundary-layer aerosol, and so the function derived from Gormley and Kennedy (1949) will be used in Sect. 6 when modelling the growth of the aerosol concentration.

Examination of the data also showed no spurious spikes in particle number when the aircraft flew in cirrus cloud, so we conclude that ice shattering on the inlet, which is an issue for large particles (McFarquhar et al., 2007), was not a significant source of particle contamination in the submicron range. This is consistent with the IAGOS D5 study (A. Petzold, personal communication, 2009) which clearly demonstrated that for this design of isokinetic inlet, ice shattering does not contaminate fine or accumulation mode aerosol measurements in cirrus clouds (but can potentially affect larger modes).

2.3 Other instruments

A complete description of the Egrett payload is given by Vaughan et al. (2008) and only those instruments whose data contributed to the present study are described here.

A SPEC Cloud Particle Imager (CPI-230) measured a wide size range of cloud particles (5–875 µm), by capturing images of ice crystals (Lawson et al., 1998) and delivering a size measurement based on the image. In this investigation, > 1 particle cm^{-3} in the 10–50 µm size range is used to define when the aircraft was in cloud. Corrections to the CPI-measured particle size distribution to account for depth of field and out-of-focus issues for small particles followed the procedures described by Connolly et al. (2007).

Carbon monoxide was measured with resonance fluorescence (Volz and Kley, 1985; Gerbig et al., 1999; Holloway et al., 2000). The instrument deployed in ACTIVE was custom-built around the fluorescence block of an AERO-Laser Model 502 CO sensor. The instrument was regularly calibrated, both on the ground and during flight. Data were collected at a frequency of 1 Hz with a precision of ± 2 ppbv and an accuracy of ± 3 ppbv (5 % at mixing ratios > 60 ppb).

Ozone was measured with a model TE-49C ultraviolet absorption spectrometer manufactured by Analytical Systems GmbH, with a response time of 10–20 s and a nominal accuracy of ± 1 ppbv. This instrument suffered some electrical interference during the flight, causing sudden changes in recorded ozone over 1 s. Fortunately, these were readily identified and removed from the data.

Three hygrometers were flown on the Egrett: one a Buck CR-2 Frost Point Hygrometer (FPH) (Busen and Buck, 1995), and the other two Tunable Diode Laser (TDL) spectrometers (May, 1998), an open-path and an in-board variant of the same basic design. The Buck and in-board TDL were the same instruments flown previously on the Egrett (Whiteway et al., 2003) while the open path instrument was new to ACTIVE. This latter instrument was added to enable humidity measurements in cloud as the inlets used for the other two did not remove cloud particles. The TDLs had a faster response time than the FPH (1 Hz compared to 0.05 Hz) but were not as accurate, while the FPH showed a very slow recovery time (several minutes) after being in cloud. In the first phase of ACTIVE (November–December 2005) the three hygrometers showed good agreement out of cloud but by January the in-board TDL had lost its calibration.

On the flight considered here the open-path TDL was measuring low, and was scaled to the FPH in a section of cloud-free air at the beginning of the flight.

The NO–NO_2 instrument deployed onboard the Egrett was a modified version of the MOZAIC NO_y instrument (Volz-Thomas et al., 2005) and is described more fully in Labrador et al. (2009). The detection limit was 200 pptv at 10 Hz and 30 pptv for an integration time of 4 s. The instrument measured either NO alone or NO and NO_2 (NO_x), and was switched between the two modes by the Egrett instrument operator. NO_x measurements only are presented here.

2.4 Data analysis

Egrett aerosol data were grouped into two nominal size ranges: 10–100 nm and 100–1000 nm, using the two CPCs. These ranges are only nominal because of the detector efficiency curves described above; that for the second CPC (with diffusion disks) in particular shows significant sensitivity to particles well below 100 nm in diameter. The 10–100 nm category was derived by subtracting the second CPC measurement (100–3000 nm) from the first (10–3000 nm). The second CPC was taken to measure from 100–1000 nm because the isokinetic inlet and curved piping are expected to have very low transmission efficiency for supermicron particles (Hermann et al., 2001). All the particle data were corrected for counting efficiency (Eq. 2) and adjusted to standard temperature pressure (STP) units (equivalent to ground level measurements).

3 Background aerosol measurements around Darwin in early 2006

Low-altitude measurements of aerosol particle concentrations were made by the CPC on the Dornier aircraft. During the active monsoon period (19–24 January) this instrument measured up to 2500 cm^{-3} of particles > 10 nm in diameter, with the vast majority of measurements < 2000 cm^{-3}. In the TTL at this time the intense convective activity meant that it was difficult to find areas of cloud-free air uninfluenced by convection

for over a day. However, the inactive monsoon which immediately followed (25 January to 3 February 2006) was free of deep convection, allowing background aerosol concentrations in the TTL to be measured.

Figure 5 summarises measurements from the two CPCs in the TTL from a flight on 3 February, away from the influence of convection. For the first CPC (> 10 nm) the median concentration was ~ 4500 cm^{-3} with maxima < 6000 cm^{-3}; for the second the corresponding values were 100 and 160 cm^{-3}. These background concentrations allow us to place the measurements that follow, taken in convective conditions, in context.

4 Nucleation case study – 23 January 2006

4.1 Flight details

On this day monsoon storms formed near the coast in the Darwin area. The Egrett took off as their anvils were beginning to dissipate; its flight path is shown in Fig. 2, and superimposed over a contemporaneous satellite image in Fig. 6. The aircraft ascended to 13 km (355 K) at 11.4° S over Bathurst Island, then flew south-west to 13.0° S, 129.4° W, retracing its path as far as 12.0° S, 130.1° W, before flying south to 13.3° S, 130.0° W, then returning via 12.5° S, 130.0° W to Darwin. The flight was designed to study the dissipating anvil over the Timor Sea, beginning in clear air then flying into cloud.

4.2 Aerosol measurements

Figure 7 shows the first 1.5 h of flight, as the aircraft ascended north-westwards over the Tiwi Islands and then flew southwest towards the anvil; at 14 h it was just off the coast of Bathurst Island. The aircraft levelled out at 13.0 h around 11 km, in saturated air with low aerosol counts, and passed through a thin cloud (yellow line) between 13.1 and 13.17 h as it began its ascent to 13 km. From 13.2 to 13.6 h LT the aircraft flew in clear air, entering cloud again at 13.66 h. In cloud, the Aitken mode aerosol counts

(orange) were low, consistent with the scavenging of aerosols and precursor gases in cloud (Twohy et al., 2002), but in the intervening clear air very high concentrations were measured (up to 28 000 cm^{-3} STP). Figure 8 shows the flight segment of Fig. 7 overlaid on the satellite image of Fig. 6. The boundary between the high and low particle number concentrations and their relation to the surrounding cloud can be clearly seen in this image.

The gas phase measurements tell a rather confusing story for this segment of flight. Firstly, NO_x concentrations of 800–1000 ppbv would normally indicate air that had recently detrained from an anvil, confirming the interpretation of the aerosol measurements – but we know from other flights that NO_x was enhanced generally in the upper troposphere around this time (Labrador et al., 2009) and there is no correlation between NO_x and relative humidity in Fig. 7. Ozone and CO both suggest a change in air mass as the aircraft entered cloud at 13.65 h, consistent with this cloud being the remnant of an anvil; lower CO and higher O_3 were both signatures of recently uplifted air on this day. As the aircraft ascended between 11 and 13 km, a gradual decrease in O_3 coincided with a similar increase in NO_x, but no change in CO. None of the tracers showed anything like the very dramatic change in humidity at 13.32 h (11.8 km) which was observed independently by all three hygrometers: relative humidity with respect to ice decreased from near-saturation to < 20 %. Although there is a local increase in both the Aitken and accumulation mode aerosol at 13.32 h, there is no consistent difference in either measurement between the near-saturated lower layer and the very dry upper layer sampled by the aircraft.

The very high concentration of small particles ($> 2 \times 10^4$ cm^{-3}) is consistent with air having recently been in cloud, followed by particle nucleation when the cloud dissipated. However, the very dry air can only be reconciled with descent: using the radiosonde profile from Garden Point on the Tiwi Islands at 14:30 LT on this day, 20 % RH is consistent with around 1.55 km of descent, 15 % with 1.85 km and 10 % with 2.25 km of descent since the air was last saturated. The lack of contrast in ozone and CO between the moist and dry sections of flight in Fig. 7 argue against long-range transport

being responsible for the dry layer, consistent with the presence of recently-nucleated aerosol, but we are unable to determine from the data we have the mechanism of local descent that this implies, other than suggesting a compensating displacement caused by injection of a fresh convective plume.

To identify possible nucleation events during this flight, regions when the Egrett was above 10 km and out of cloud were divided into 5 km sections. The criterion for identifying possible nucleation events was taken to be $\geq$ 2000 Aitken mode particles cm^{-3}; this latter value exceeded boundary-layer measurements made by the Dornier during this period thus excluding any direct boundary-layer source for the observed particles. The flight track was superimposed on to the closest MTSAT satellite image in time (infrared channel 2, 11.5–12 µm); i.e. to the nearest half hour (since MTSAT data were recorded hourly). Allowance was made for the 20 min taken for the MTSAT scan to reach the Darwin area.

4.3 Interpretation of nucleation events

Having identified recent nucleation events, we now turn to the question of time scale – how long was it since the air was last in cloud? To answer this question we use the winds measured on board the Egrett to project air parcels back in time for up to 5 h, at constant height. The assumption of constant height is obviously incorrect for the dry layer in Fig. 7, so the analysis that follows is restricted to points where the relative humidity over ice exceeded 70 %, corresponding to a maximum descent since air exited cloud of 500 m. Winds were derived from a combination of a Rosemount 5-hole probe and pressure transducers, a Trimble TANS Vector GPS attitude system and a Novatel 12-channel GPS receiver. A check on the validity of back-projection at constant height was obtained by comparing the calculations with back-trajectories calculated using the British Atmospheric Data Centre (BADC) trajectory server, based on ECMWF analysis at a resolution of 2.5 × 2.5° (for further details see Allen et al., 2009).

Wind projections were initiated from the centre of the 5 km flight sections under investigation, using 50 s (∼ 5 km) median averages of the 1 s winds. The location of

the trajectories relative to cloud was evaluated by comparison with MTSAT infra-red images. The median value of IR brightness temperature (11.5–12.5 µm) was calculated over a 5 km radius, at the end points of the trajectories. This was converted to height using a radiosonde profile measured from a ship located near the Egrett path at 14:27 LT (Fig. 6).

Figure 9 shows an example of the variation of cloud brightness temperature (left panel) derived along a trajectory. The corresponding cloud top height is shown in the right panel. We define the time at which the trajectory exited cloud as the point where the derived cloud top height is equal to the aircraft height – in this case 11.2 km, corresponding to a time of around 2.3 h since the air was last in cloud. This methodology was applied to all the data segments.

For the wind data, uncertainties were estimated by the standard deviation of the wind velocity vectors within the 5 km segments. Since the MTSAT satellite scanned hourly, further uncertainty was introduced by the time resolution available in the IR images. These errors were combined to provide an uncertainty in the outflow time.

5 Results

Of the 115 data segments with $\geq$ 2000 Aitken nuclei cm^{-3}, 67 could be analysed using the methodology above. The other 48 occurred below higher-level cloud, so the evolution of cloud top height along trajectories could not be used. For the 67 analysed cases, median particle number concentration is shown as a function of the time since the parent cloud evaporated, in Fig. 10. The sensitivity of the result was tested by adding a +5 K and a −5 K offset to the temperature-altitude relationship. This allows for the possibility of descent along the trajectories of up to 500 m, as well as other positional errors.

The Aitken mode aerosol (10–100 nm) reached a concentration of $>$ 20 000 cm^{-3} after 3–4 h, and stayed at that level for the next 2–3 h. Loss mechanisms, such as coagulation, reduce the aerosol population over time, as nucleation and sulphuric acid

production rates drop (Clement et al., 2002, 2006). The accumulation mode (nominally 100–1000 nm) shows a different pattern; the exponentially fitted trendlines indicate a rapid growth in number concentration between 4 and 6 h. In fact, these counts arise from Aitken mode particles (20–30 nm) detected because of the broad efficiency cut-off imposed by the diffusion disks. The increase over time indicates a gradual shift in the size distribution, bringing more particles into the detectable size range. This point is examined in more detail below.

6 Discussion

We examine here the hypothesis that the storm anvil outgassed SO_2 (from the PBL and/or entrained in the mid and upper troposphere) which was oxidised by OH (Ekman et al., 2006) and further reacted with water and oxygen to produce sulphuric acid. Sulphuric acid and water molecules then formed clusters, leading to aerosol nucleation and growth.

On the face of it, the results of Fig. 10 are not inconsistent with the modelling study of Clement et al. (2006): the concentration of aerosol >20 nm in diameter in Fig. 1 reaches $10^4\,cm^{-3}$ in 3–4 h, compared to a similar concentration after ~ 2 h in the (>10 nm) measured particles. On closer examination however, agreement is not so good. Clement et al. (2006) assumed an SO_2 concentration of 1 ppbv, leading to an H_2SO_4 production rate of $10^5\,cm^{-3}\,s^{-1}$. Such a concentration is very unlikely to have occurred in the Darwin area, as we now argue.

Background concentrations of SO_2 in the tropics above 10 km are below 100 pptv (English et al., 2011; Fiedler et al., 2011), but concentrations can be greatly enhanced in plumes from combustion sources (e.g., Fiedler et al., 2011). Six-day back-trajectories from the flight segment in Fig. 7, calculated using the on-line HYSPLIT model, showed that the air originated either to the north-east (over New Guinea) or remained over the Northern Territory. The MODIS fire map for the period 22–30 January 2006 (Fig. 11) shows that the nearest significant biomass burning was in Borneo and Sumatra, far to the west of the back-trajectory end-points. Together with the measured

CO concentration of 50–55 ppbv, this rules out a biomass burning component to the sampled air mass.

The nearest SO_2 measurements in time to this flight were those from the SCOUT-O3 campaign in November-December 2005 (Vaughan et al., 2008), on the Falcon aircraft using Ion Trap mass spectrometry (Speidel et al., 2007). A total of 9 FALCON missions took place from Darwin during the period 16 November–9 December 2005, including several penetrations of deep convective anvils; for details see Fiedler et al. (2011). Figure 12 shows altitude profiles of SO_2 measured on all 9 flights. In the upper troposphere, mean values were usually below 110 pptv, 75 % percentile values below 150 pptv, and 90 % percentile values below 160 pptv; excess SO_2 was observed only on two occasions in two thin layers (up to 270 and 380 pptv) whose origins were not identified. Ten-day back-trajectories from the air masses probed by the FALCON indicate that above 10 km, upper tropospheric SO_2 was mostly influenced by the Indonesian boundary layer. Biomass burning was reducing in intensity during the SCOUT-O3 campaign, consistent with the observed decrease in SO_2 (Fig. 12). As, there was no biomass burning in the Darwin area during the active monsoon in January, it is very unlikely that the SO_2 concentration on 23 January 2006 exceeded that in December, and 100 pptv is taken as the maximum conceivable SO_2 concentration during the flight considered here.

For an estimate of OH, we first take the median upper tropospheric OH concentration of 0.23 pptv measured by the STRAT campaign (flown over the North Pacific between 1995 and 1996, at an average latitude of 22° N, Jaeglé et al., 2001). Using the H_2SO_4 production rate of Clement et al. (2006):

$$P = 10^{-18}[OH][SO_2]\,m^{-3}\,s^{-1}, \quad (3)$$

with 0.23 pptv OH (1.5×10^6 molecules cm^{-3}) and 100 pptv of SO_2 at a pressure of 200 hPa and temperature of 223 K gives $P \sim 1000\,cm^{-3}\,s^{-1}$. This is much lower than the $10^5\,cm^{-3}\,s^{-1}$ used in Clement et al. (2006).

An alternative estimate of OH may be found using a global chemical transport model calculation for the time and place of the measurement. An estimate from the p-TOMCAT model run for the ACTIVE campaign (O. Dessens, personal communication 2009) gave 0.4 pptv at 208 hPa in the middle of the day. The corresponding relative humidity of 30 % with respect to ice is likely to be an underestimate in air that has recently exited an anvil, so a mixing ratio nearer to 1 pptv may be more appropriate in these conditions. This would imply an SO_2 destruction rate of 4220 cm^{-3} s^{-1} (assuming 100 pptv of SO_2).

A simple test of the above hypothesis can be made by estimating the number of sulphuric acid molecules in the measured aerosol and comparing with the total production derived using P above. Boy et al. (2008) estimate that a nucleation mode (< 10 nm) particle is typically composed of 5–30 % sulphuric acid by mass; this ratio is expected to fall as the particles grow into the Aitken mode. For the purposes of this test, the 10–100 nm size range is assumed to contain 25 % sulphuric acid by mass. The minimum amount of sulphur that could could be contained in the measured aerosol is calculated by assuming a monodisperse aerosol size distribution with the smallest detectable diameter of 10 nm. Maximum aerosol concentrations were ∼ 25 000 cm^{-3} (STP), corresponding to 6570 cm^{-3} in situ. This gives a sulphuric acid concentration of 5.9×10^6 molecules cm^{-3}. For a production rate of 4220 cm^{-3} s^{-1}, this concentration would be achieved in 23 min, well within the timescale implied by Fig. 10.

The aerosol is not monodispere however, so a more detailed calculation was performed assuming a lognormal aerosol size distribution, with a standard deviation of 1.237 nm derived from the curves in Fig. 1. Detector efficiency curves were taken from Eq. (1) for the unmodified CPC, and from Feldpausch et al. (2006) at 200 hPa for that with diffusion disks. To simulate the results of Fig. 10 a linear growth rate was assumed for the particles. The timescale for the observed particle number to reach a maximum in this simple model depends only on the growth rate; the actual maximum number is then a function of the H_2SO_4 production rate. The latter was calculated with a fixed OH concentration of 1 pptv and variable SO_2 concentration.

It was found that the observed growth in particle number to 25 000 cm^{-3} (STP) after 3–4 h (Fig. 10) was best simulated with an SO_2 concentration of 50 pptv and a linear growth in the mode of the lognormal distribution from 5 nm (diameter) at 1 h to 19 nm after 5 h. This result may be compared with the analytical formulae presented by Clement et al. (2006) for aerosol particle growth which show that a H_2SO_4 production rate of 4×10^4 cm^{-3} s^{-1} is required to match the inferred growth rate – implying an SO_2 concentration of 1 ppbv. The hypothesis that SO_2 oxidation is the source of the particles would not therefore appear to be consistent with the observed particle growth rate.

Evidence that some particles grew to the 20–30 nm range after 5 h comes from the CPC with diffusion disks. Using the same calculation as above, with a particle size distribution whose mode increases linearly with time to 19 nm after 5 h, and multiplying by the detector efficiency curve of Feldpausch et al. (2006), the rapid growth in "accumulation mode" aerosol could be reproduced fairly well. Given the uncertainty in the exact shape of this efficiency curve, little quantitative information about the aerosol could be derived from this CPC, but the rapid increase in measured particles is a strong qualitative indication that some particles are indeed reaching sizes of tens of nm over this time scale.

To examine these processes further, simulations of aerosol nucleation and growth were made using the AEROFOR model presented by Pirjola and Kulmala (1998). The model uses a 27 section representation of the aerosol distribution, from 0.5×10^{-9} m to 1.0×10^{-6} m, and fully represents nucleation, condensational growth and coagulation using sulphuric acid as the primary condensable. We present results using an SO_2 concentration of 100 pptv and an OH concentration of 0.8 pptv, double the p-TOMCAT estimate, to correspond to the maximum possible H_2SO_4 production rate. Because of the short time since detrainment of the anvil, we neglect dilution of the plume by entrainment of ambient air.

The OH concentration was modulated with a semi-sinusoidal function to replicate the variation of sunlight intensity during daylight hours, with simulations commencing

6 h after sunrise since most convective activity intensified around noon local time. Sulphuric acid and total aerosol concentration (> 0.5 nm) increase rapidly to a maximum within 2–4 h (right, Fig. 13), as nucleation begins. The sulphuric acid concentration then drops as the acid condenses onto the ever larger population of particles; the total particle concentration also decreases due to the coagulation of smaller particles into larger. A large nucleation mode exists up to 5 h (see 0.5, 1, 2 and 5 h curves); the emergence of the Aitken mode is not evident until 8 h, when a "shoulder" appears in the size distribution.

The bold dotted line in Fig. 13 shows the expected counts from the unmodified CPC, calculated by multiplying the aerosol size distribution at a given time with the instrument efficiency curve, equation 1, and the pipework transmission function. Expected concentrations after 5 h are $\sim 500\,cm^{-3}$ – much less than observed despite the upper limit assumed on the sulphuric acid production rate. This (together with the observed increase in signal on the second CPC) suggests that the model seriously underestimates the growth of particles to the observable size range. Thus, the hypothesis that SO_2 outgassed from the storm is responsible for the observed particle concentrations is only tenable if coagulation rates in the model are grossly underestimated.

This discrepancy between measurements and theory could be resolved if there was another source of condensable material, e.g. organic compounds (Loukonen et al., 2010). A range of such compounds were measured on the Dornier during ACTIVE using a tube sampler followed by off-line gas chromatography (Allen et al., 2008). Total concentrations of organics of order 1 ppbv were measured in the boundary layer between 20 and 27 January, which could have resulted in sufficient condensable material in the storm outflow, once the H_2SO_4 had nucleated new particles.

Ion–assisted nucleation (Yu and Turco, 2001) could increase the rate at which particles were formed, but does not explain why too few particles in the model grow to the observable range. We note also that the role of ions in nucleating particles in the atmosphere is still a matter of debate – e.g., Kulmala et al. (2010); Kirkby et al. (2011).

7 Conclusions

This study has found that air that recently exited the outflow of a convective storm in the tropics contained much higher Aitken mode aerosol concentrations than in the boundary layer or in the anvil cloud. Inside cloud, the concentration of aerosol in the size range 10–100 nm were $< 100\,cm^{-3}$; downwind of the cloud, concentrations were as high as $25\,000\,cm^{-3}$ STP. The upper troposphere CARIBIC study (Heintzenberg et al., 2003) found concentrations of 10 000–30 000 cm^{-3} (STP) for aerosol of diameter 4–12 nm, and $9000\,cm^{-3}$ (STP) for the 12–18 nm size range. Twohy et al. (2002) reported concentrations up to $45\,000\,cm^{-3}$ for sizes ≥ 20 nm downwind of a mid-latitude mesoscale storm. The present results are intermediate between these two, with Aitken mode particles (10–100 nm) up to $25\,000\,cm^{-3}$ (STP).

Using the wind measurements on board the Egrett together with infra-red satellite images, a time scale of 3–4 h is deduced for observable aerosol (> 10 nm diameter) to reach $\sim 25\,000\,cm^{-3}$ (STP), after air has exited a convective anvil. In addition, there is clear evidence from the particle counter with diffusion disks of particle growth to the 20–30 nm range over a period of 4–6 h. Simple estimates of sulphuric acid availability, based on measurements of SO_2 in the first phase of the ACTIVE campaign and OH estimates from a global model, suggest that sufficient acid could have been present to explain these observations. However, a detailed model of aerosol nucleation and growth was unable to produce sufficient numbers of particles > 10 nm over the requisite time scale. This suggests either that models of aerosol coagulation in the upper troposphere need to be revised, or that substances other than sulphuric acid (e.g. organics) contribute to aerosol condensation and growth in the TTL.

Acknowledgements. We thank the pilots and ground crew of the Egrett and Dornier aircraft for ensuring a successful campaign, and to Peter May and the staff of the Bureau of Meteorology (BoM) Regional Centre in Darwin for their support in forecasting and logistics. We thank also Marcel Berg and Norbert Houben for maintenance of the CO instrument, and the Royal Australian Air Force for hosting the aircraft experiment. Olivier Dessens provided the OH estimates from the p-TOMCAT model. Finally, we thank the UK Natural Environment Research Council

(Grant NE/C512688/1) and NERC Airborne Remote Sensing Facility for supporting ACTIVE. DW is a NERC-supported research student.

References

Allen, G., Vaughan, G., Bower, K., Williams, P., Crosier, J., Flynn, M., Connolly, P., Hamilton, J., Lee, J., Saxton, J., Watson, N., Gallagher, M., Coe, H., Choularton, T. W., Allan, J., and Lewis, A.: Aerosol and trace-gas measurements in the Darwin area during the wet season, J. Geophys. Res., 113, D06306, doi:10.1029/2007JD008706, 2008. 2360, 2362, 2373

Allen, G., Vaughan, G., Brunner, D., May, P. T., Heyes, W. Minnis, P., and Ayres, J. K.: Modulation of tropical convection by breaking Rossby waves, Q. J. Roy. Meteor. Soc., 135, 125–137, 2009. 2367

Andreae, M. O., Artaxo, P., Fischer, H., Freitas, S. R., Gregoire, J. M., Hansel, A., Hoor, P., Kormann, R., Krejci, R., Lange, L., Lelieveld, J., Lindinger, W., Longo, K., Peters, W., de Reus, M., Scheeren, B., Dias, M. A. F. S., Strom, J., van Velthoven, P. F. J., and Williams, J.: Transport of biomass burning smoke to the upper troposphere by deep convection in the tropical region, Geophys. Res. Lett., 28, 951–954, 2001. 2358

Borrmann, S., Kunkel, D., Weigel, R., Minikin, A., Deshler, T., Wilson, J. C., Curtius, J., Volk, C. M., Homan, C. D., Ulanovsky, A., Ravegnani, F., Viciani, S., Shur, G. N., Belyaev, G. V., Law, K. S., and Cairo, F.: Aerosols in the tropical and subtropical UT/LS: in-situ measurements of submicron particle abundance and volatility, Atmos. Chem. Phys., 10, 5573–5592, doi:10.5194/acp-10-5573-2010, 2010. 2357

Boy, M., Karl, T., Turnipseed, A., Mauldin, R. L., Kosciuch, E., Greenberg, J., Rathbone, J., Smith, J., Held, A., Barsanti, K., Wehner, B., Bauer, S., Wiedensohler, A., Bonn, B., Kulmala, M., and Guenther, A.: New particle formation in the Front Range of the Colorado Rocky Mountains, Atmos. Chem. Phys., 8, 1577–1590, doi:10.5194/acp-8-1577-2008, 2008. 2359, 2371

Brenninkmeijer, C. A. M., Crutzen, P., Boumard, F., Dauer, T., Dix, B., Ebinghaus, R., Filippi, D., Fischer, H., Franke, H., Frieß, U., Heintzenberg, J., Helleis, F., Hermann, M., Kock, H. H., Koeppel, C., Lelieveld, J., Leuenberger, M., Martinsson, B. G., Miemczyk, S., Moret, H. P., Nguyen, H. N., Nyfeler, P., Oram, D., O'Sullivan, D., Penkett, S., Platt, U., Pupek, M., Ramonet, M., Randa, B., Reichelt, M., Rhee, T. S., Rohwer, J., Rosenfeld, K., Scharffe, D.,

Schlager, H., Schumann, U., Slemr, F., Sprung, D., Stock, P., Thaler, R., Valentino, F., van Velthoven, P., Waibel, A., Wandel, A., Waschitschek, K., Wiedensohler, A., Xueref-Remy, I., Zahn, A., Zech, U., and Ziereis, H.: Civil Aircraft for the regular investigation of the atmosphere based on an instrumented container: The new CARIBIC system, Atmos. Chem. Phys., 7, 4953–4976, doi:10.5194/acp-7-4953-2007, 2007. 2357

Brock, C. A., Hamill, P., Wilson, J. C., Jonsson, H. H., and Chan, K. R.: Particle formation in the upper tropical troposphere – a source of nuclei for the stratospheric aerosol, Science, 270, 1650–1653, 1995. 2357

Busen, R. and Buck, A. L.: A high-performance hygrometer for aircraft use: description, installation and flight data, J. Atmos. Ocean. Techn., 12, 73–84, 1995. 2363

Choularton, T. W., Bower, K. N., Weingartner, E., Crawford, I., Coe, H., Gallagher, M. W., Flynn, M., Crosier, J., Connolly, P., Targino, A., Alfarra, M. R., Baltensperger, U., Sjogren, S., Verheggen, B., Cozicb, J., and Gysel, M.: The influence of small aerosol particles on the properties of water and ice clouds, Faraday Discuss., 137, 205–222, 2008. 2356

Clement, C. F., Ford, I. J., Twohy, C. H., Weinheimer, A., and Campos, T.: Particle production in the outflow of a midlatitude storm, J. Geophys. Res., 107, 4559, doi:10.1029/2001JD001352, 2002. 2357, 2358, 2369

Clement, C. F., Pirjola, L., Twohy, C. H., Ford, I. J., Kulmala, M.: Analytic and numerical calculations of the formation of a sulphuric acid aerosol in the upper troposphere, J. Aerosol Sci., 37, 1717–1729, 2006. 2359, 2369, 2370, 2372, 2382

Connolly, P. J., Flynn, M. J., Ulanowski, Z., Choularton, T. W., Gallagher, M. W., and Bower, K. N.: Calibration of the cloud particle imager probes using calibration beads and ice crystal analogs: the depth of field, J. Atmos. Ocean. Tech., 24, 860–1879, 2007. 2363

Ekman, A. M. L., Wang, C., Ström, J., and Krejki, R.: Explicit simulation of aerosol physics in a cloud-resolving model: aerosol transport and processing in the free troposphere, J. Atmos. Sci., 63, 682–696, 2006. 2369

English, J. M., Toon, O. B., Mills, M. J., and Yu, F.: Microphysical simulations of new particle formation in the upper troposphere and lower stratosphere, Atmos. Chem. Phys., 11, 9303–9322, doi:10.5194/acp-11-9303-2011, 2011. 2369

Feldpausch, P., Fiebig, M., Fritzsche, L., and Petzold, A.: A Measurement of ultrafine size distributions by a combination of diffusion screen separators and condensation particle counters, J. Aerosol Sci., 37, 577–597, 2006. 2361, 2371, 2372

Fiedler, V., Nau, R., Ludmann, S., Arnold, F., Schlager, H., and Stohl, A.: East Asian SO_2

pollution plume over Europe – Part 1: Airborne trace gas measurements and source identification by particle dispersion model simulations, Atmos. Chem. Phys., 9, 4717–4728, doi:10.5194/acp-9-4717-2009, 2009. 2358

Fiedler, V., Arnold, F., Ludmann, S., Minikin, A., Hamburger, T., Pirjola, L., Dörnbrack, A., and Schlager, H.: African biomass burning plumes over the Atlantic: aircraft based measurements and implications for H_2SO_4 and HNO_3 mediated smoke particle activation, Atmos. Chem. Phys., 11, 3211–3225, doi:10.5194/acp-11-3211-2011, 2011. 2358, 2369, 2370

Füglistaler, S., Dessler, A. E., Dunkerton, T. J., Folkins, I., Fu, Q., and Mote, P. W.: The tropical tropopause layer, Rev. Geophys., 47, RG1004, doi:10.1029/2008RG000267, 2009. 2356

Gallagher, M. W., Connolly, P. J., Whiteway, J., Figueras-Nieto, D., Flynn, M., Choularton, T. W., Bower, K. N., Cook, C., Busen, R., and Hacker, J.: An overview of the microphysical structure of cirrus clouds observed during EMERALD-1, Q. J. Roy. Meteor. Soc., 131, 1143–1169, 2005. 2356

Gerbig, C., Schmitgen, S., Kley, D., Volz-Thomas, A., Dewey, K., and Haaks, D.: An improved fast-response vacuum-UV fluorescence CO instrument, J. Geophys. Res., 104, 1699–1704, 1999. 2363

Gormley, P. G. and Kennedy, M.: Diffusion from a stream flowing through a cylindrical tube, P. Roy. Irish Acad. A, 52, 163–169, 1949. 2362

Heintzenberg, J., Hermann, M., and Theiss, D.: Out of Africa: High aerosol concentrations in the upper troposphere over Africa, Atmos. Chem. Phys., 3, 1191–1198, doi:10.5194/acp-3-1191-2003, 2003. 2357, 2374

Hermann, M., Stratmann, F., Wilck, F., and Wiedensohler, A.: Sampling characteristics of an aircraft-borne aerosol inlet system, J. Atmos. Ocean. Tech., 18, 7–19, 2001. 2361, 2364

Hermann, M., Heintzenberg, J., Wiedensohler, A., Zahn, A., Heinrich, G., and Brenninkmeijer, C. A. M.: Meridional distributions of aerosol particle number concentrations in the upper troposphere and lower stratosphere obtained by Civil Aircraft for Regular Investigation of the Atmosphere Based on an Instrument Container (CARIBIC) flights, J. Geophys. Res., 108, 4114, doi:10.1029/2001JD001077, 2003. 2357

Hermann, M., Brenninkmeijer, C. A. M., Slemr, F., Heintzenberg, J., Martinsson, B. G., Schlager, H., van Velthoven, P. F. J., and Wiedensohler, A.: Submicrometer aerosol particle distributions in the upper troposphere over the mid-latitude North Atlantic – results from the third route of "CARIBIC", Tellus B, 60, 106–117, 2008. 2357

Heyes, W. J., Vaughan, G., Allen, G., Volz-Thomas, A., Pätz, H.-W., and Busen, R.: Composi-

tion of the TTL over Darwin: local mixing or long-range transport?, Atmos. Chem. Phys., 9, 7725–7736, doi:10.5194/acp-9-7725-2009, 2009.

Holloway, J. S., Jakoubek, R. O., Parrish, D. D., Gerbig, C., Volz-Thomas, A., Schmitgen, S., Fried, A., Wert, B. H. B., and Drummond, J. R.: Airborne intercomparison of vacuum ultraviolet fluorescence and tunable diode laser absorption measurements of tropospheric carbon monoxide, J. Geophys. Res., 105, 24251–24262, 2000. 2363

Jaeglé, L., Jacob, D. J., Brune, W. H., and Wennberg, P. O.: Chemistry of HO_x radicals in the upper troposphere, Atmos. Environ., 35, 469–489, 2001. 2370

Kirkby, J., Curtius, J., Almeida, J., Dunne, E., Duplissy, J., Ehrhart, S., Franchin, A., Gagné, S., Ickes, L., Kürten, A., Kupc, A., Metzger, A., Riccobono, F., Rondo, L., Schobesberger, S., Tsagkogeorgas, G., Wimmer, D., Amorim, A., Bianchi, F., Breitenlechner, M., David, A., Dommen, J., Downard, A., Ehn, M., Flagan, R. C., Haider, S., Hansel, A., Hauser, D., Jud, W., Junninen, H., Kreissl, F., Kvashin, A., Laaksonen, A., Lehtipalo, K., Lima, J., Lovejoy, E. R., Makhmutov, M., Mathot, S., Mikkilä, J., Minginette, P., Mogo, S., Nieminen, T., Onnela, A., Pereira, P., Petäjä, T., Schnitzhofer, R., Seinfeld, J. H., Sipilä, M., Stozhkov, Y., Stratmann, F., Tomé, A., Vanhanen, J., Viisanen, Y., Vrtala, A., Wagner, P. E., Walther, H., Weingartner, E., Wex, H., Winkler, P. M., Carslaw, K. S., Worsnop, D. R., Baltensperger, U., and Kulmala, M.: Role of sulphuric acid, ammonia and galactic cosmic rays in atmospheric aerosol nucleation, Nature, 476, 429–433, 2011. 2373

Kulmala, M., Reissell, A., Sipilä, M., Bonn, B., Ruuskanen, T. M., Lehtinen, K. E. J., Kerminen, V.-M., and Ström, J.: Deep convective clouds as aerosol production engines: role of insoluble organics, J. Geophys. Res., 111, D17202, doi:10.1029/2005JD006963, 2006. 2358, 2359

Kulmala, M., Riipinen, I., Nieminen, T., Hulkkonen, M., Sogacheva, L., Manninen, H. E., Paasonen, P., Petäjä, T., Dal Maso, M., Aalto, P. P., Viljanen, A., Usoskin, I., Vainio, R., Mirme, S., Mirme, A., Minikin, A., Petzold, A., Hõrrak, U., Plaß-Dũlmer, C., Birmili, W., and Kerminen, V.-M.: Atmospheric data over a solar cycle: no connection between galactic cosmic rays and new particle formation, Atmos. Chem. Phys., 10, 1885–1898, doi:10.5194/acp-10-1885-2010, 2010. 2373

Laakso, L., Mäkelä, J. M., Pirjola, L., and Kulmala, M.: Model studies on ion-induced nucleation in the atmosphere, J. Geophys. Res., 107, 4427, doi:10.1029/2002JD002140, 2002. 2358

Laakso, L., Kulmala, M., and Lehtinen, K. E. J.: Effect of condensation rate enhancement factor on 3-nm (diameter) particle formation in binary ion-induced and homogeneous nucleation,

J. Geophys. Res., 108, 4574, doi:10.1029/2003JD003432, 2003. 2359
Laakso, L., Gagnń, S., Petäjä, T., Hirsikko, A., Aalto, P. P., Kulmala, M., and Kerminen, V.-M.: Detecting charging state of ultra-fine particles: instrumental development and ambient measurements, Atmos. Chem. Phys., 7, 1333–1345, doi:10.5194/acp-7-1333-2007, 2007. 2359
Labrador, L., Vaughan, G., Heyes, W., Waddicor, D., Volz-Thomas, A., Pätz, H.-W., and Höller, H.: Lightning-produced NO_x during the Northern Australian monsoon; results from the ACTIVE campaign, Atmos. Chem. Phys., 9, 7419–7429, doi:10.5194/acp-9-7419-2009, 2009. 2364, 2366
Lee, S.-H., Wilson, J. C., Baumgardner, D., Herman, R. L., Weinstock, E. M., LaFleur, B. G., Kok, G., Anderson, B., Lawson, P., Baker, B., Strawa, A., Pittman, J. V., Reeves, J. M., and Bui, T. P: New particle formation observed in the tropical/subtropical cirrus clouds, J. Geophys. Res., 109, D20209, doi:10.1029/2004JD005033, 2004.
Lawson, R. P., Heymsfield, A. J., Aulenbach, S. M., and Jensen, T. L.: Shapes, sizes and light scattering properties of ice crystals in cirrus and a persistent contrail during SUCCESS, Geophys. Res. Lett., 25, 1331–1334, 1998. 2363
Loukonen, V., Kurtén, T., Ortega, I. K., Vehkamäki, H., Pádua, A. A. H., Sellegri, K., and Kulmala, M.: Enhancing effect of dimethylamine in sulfuric acid nucleation in the presence of water – a computational study, Atmos. Chem. Phys., 10, 4961–4974, doi:10.5194/acp-10-4961-2010, 2010. 2373
McFarquhar, G. M., Um, J., Freer, M., Baumgardner, D., Kok, G. L., and Mace, G. G.: Importance of small ice crystals to cirrus properties: observations from the Tropical Warm Pool International Cloud Experiment (TWP-ICE), Geophys. Res. Lett., 34, L13803, doi:10.1029/2007GL029865, 2007. 2362
May, R. D.: Open-path, near-infrared tunable diode laser spectrometer for atmospheric measurements of H_2O, J. Geophys. Res., 103, 19161–19172, 1998. 2363
May, P. T., Mather, J. H., Vaughan, G., Jakob, C., McFarquhar, G. M., Bower, K. N., and Mace, G. G.: The Tropical Warm Pool International Cloud Experiment (TWP-ICE), B. Am. Meteorol. Soc., 89, 632–645, 2008. 2360
Möhlerr, O. and Arnold, F.: Gaseous sulfuric acid and sulfur dioxide measurements in the troposphere and lower stratosphere: implications for hydroxyl radical abundances. Geophys. Res. Lett., 19, 1763–1766, 1992. 2358
Perry, K. D., and Hobbs, P. V.: Further evidence for particle nucleation in clear air adjacent to

marine cumulus clouds, J. Geophys. Res., 99, 22803–22818, 1994. 2358
Pirjola, L. and Kulmala, M.: Modelling the formation of H_2SO_4–H_2O particles in rural, urban and marine conditions, Atmos. Res., 46, 321–347, 1998. 2372
Schröder, F. and Ström, J.: Aircraft measurements of sub micrometer aerosol particles (> 7 nm) in the midlatitude free troposphere and tropopause region, Atmos. Res., 44, 333–356, 1997. 2357
Ström, J., Fischer, H., Lelieveld, J., and Schröder, F.: In situ measurements of microphysical properties and trace gases in two cumulonimbus anvils over Western Europe, J. Geophys. Res., 104, 12221–12226, 1999. 2358
Seifert, M., Ström, J., Krejci, R., Minikin, A., Petzold, A., Gayet, J.-F., Schlager, H., Ziereis, H., Schumann, U., and Ovarlez, J.: Aerosol-cirrus interactions: a number based phenomenon at all?, Atmos. Chem. Phys., 4, 293–305, doi:10.5194/acp-4-293-2004, 2004a.
Seifert, M., Tiede, R., Schnaiter, M., Linke, C., Möhler, O., Schurath, U., and Ström, J.: Operation and performance of a differential mobility particle sizer and a TSI 3010 condensation particle counter at stratospheric temperatures and pressures, J. Aerosol Sci. 35, 81, 2004b. 2356
2361
Sihto, S.-L., Kulmala, M., Kerminen, V.-M., Dal Maso, M., Petäjä, T., Riipinen, I., Korhonen, H., Arnold, F., Janson, R., Boy, M., Laaksonen, A., and Lehtinen, K. E. J.: Atmospheric sulphuric acid and aerosol formation: implications from atmospheric measurements for nucleation and early growth mechanisms, Atmos. Chem. Phys., 6, 4079–4091, doi:10.5194/acp-6-4079-2006, 2006. 2359
Smith, J. A., Ackerman, A. S., Jensen, E. R., and Toon, O. B.: Role of deep convection in establishing the isotopic composition of water vapor in the tropical transition layer, Geophys. Res. Lett., 33, L06812, doi:10.1029/2005GL024078, 2006.
Speidel, M., Nau, R., Arnold, F., Schlager, H., and Stohl, A.: Sulfur dioxide measurements in the lower, middle and upper troposphere: deployment of an aircraft-based chemical ionization mass spectrometer with permanent in-flight calibration, Atmos. Environ., 41, 2427–2437, 2007. 2370
Twohy, C. H., Clement, C. F., Gandrud, B. W., Weinheimer, A. J., Campos, T. L., Baumgardner, D., Brune, W. H., Faloona, I., Sachse, G. W., Vay, S. A., and Tan, D.: Deep convection as a source of new particles in the midlatitude upper troposphere, J. Geophys. Res., 107, 4560, doi:10.1029/2001JD000323, 2002. 2357, 2358, 2366, 2374

Vaughan, G., Schiller, C., MacKenzie, A. R., Bower, K., Peter, T., Schlager, H., Harris, N. R. P., and May, P. T.: SCOUT-O3 /ACTIVE: high-altitude aircraft measurements around deep tropical convection, B. Am. Meteorol. Soc., 89, 647–662, 2008. 2360, 2362, 2370

Volz, A. and Kley, D.: A resonance fluorescence instrument for the in-situ measurement of atmospheric carbon monoxide, J. Atmos. Chem., 2, 345–357, 1985. 2363

Volz-Thomas, A., Berg, M., Heil, T., Houben, N., Lerner, A., Petrick, W., Raak, D., and Pätz, H.-W.: Measurements of total odd nitrogen (NO_y) aboard MOZAIC in-service aircraft: instrument design, operation and performance, Atmos. Chem. Phys., 5, 583–595, doi:10.5194/acp-5-583-2005, 2005. 2364

Wang, C.: A modeling study of the response of tropical deep convection to the increase of cloud condensation nuclei concentration: 1. Dynamics and microphysics, J. Geophys. Res., 110, D21211, doi:10.1029/2004JD005720, 2005a. 2356

Wang, C.: A modeling study of the response of tropical deep convection to the increase of cloud condensation nuclei concentration: 2. Radiation and tropospheric chemistry, J. Geophys. Res., 110, D22204, doi:10.1029/2005JD005829, 2005b. 2356

Weigel, R., Borrmann, S., Kazil, J., Minikin, A., Stohl, A., Wilson, J. C., Reeves, J. M., Kunkel, D., de Reus, M., Frey, W., Lovejoy, E. R., Volk, C. M., Viciani, S., D'Amato, F., Schiller, C., Peter, T., Schlager, H., Cairo, F., Law, K. S., Shur, G. N., Belyaev, G. V., and Curtius, J.: In situ observations of new particle formation in the tropical upper troposphere: the role of clouds and the nucleation mechanism, Atmos. Chem. Phys., 11, 9983–10010, doi:10.5194/acp-11-9983-2011, 2011. 2357

Whiteway, J. A., Cook, C., Gallagher, M., Choularton, T. W., Harries, J., Connolly, P., Busen, R., Bower, K. N., Flynn, M., May, P. T., Aspey, R., and Hacker, J.: Anatomy of cirrus clouds: results from the Emerald airborne campaigns, Geophys. Res. Lett., 31, L24102, doi:10.1029/2004GL021201, 2004. 2363

Wiedensohler, A., Orsini, D., Covert, D. S., Coffmann, D., Cantrell, W., Havlicek, M., Brechtel, F. J., Russell, L. M., Weberg, R. J., Gras, J., Hudson, J. G., and Litchy, M.: Intercomparison study of the size-dependent counting efficiency of 26 condensation particle counters, Aerosol Sci. Tech., 27, 224–242, 1997. 2361

Yu, F. and Turco, R. P.: From molecular clusters to nanoparticles: role of ambient ionization in tropospheric aerosol formation, J. Geophys. Res., 106, 4797–4814, 2001. 2358, 2373

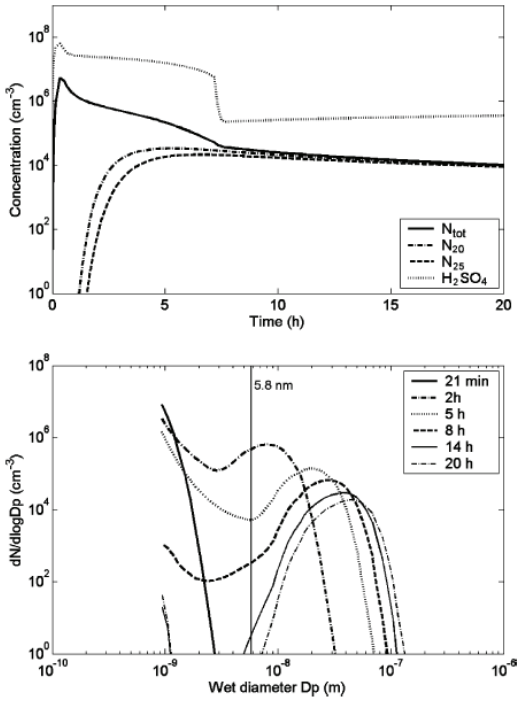

Fig. 1. Numerical calculations of size distribution with time. The top figure shows the change of concentration with time for a given size range: the legend for the curves shows N_{tot} as the total aerosol concentration (greater than 3 nm), N_{20} the concentration greater than 20 nm, N_{25} greater than 25 nm and H_2SO_4 as the acid production rate. The lower figure shows the size distribution of the aerosol and the various curves represent the distribution at a given time. The legend indicates 21 min, 2, 5, 8, 14 and 20 h (h). Figure from Clement et al. (2006).

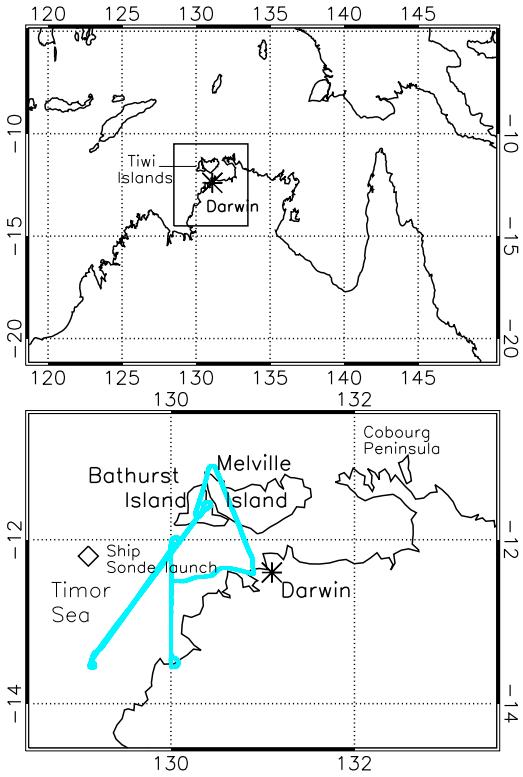

Fig. 2. Top: Northern Australia (cutout shown in bottom image); bottom: a blow-up of the Darwin-Tiwi Island region – focus of the ACTIVE project. The light blue line indicates the flight path of the ARA Egrett aircraft on 23 January 2006.

Fig. 3. Port pylon of the Egrett. In the foreground is the CAPS probe; above and to the left (as viewed), is the aerosol inlet.

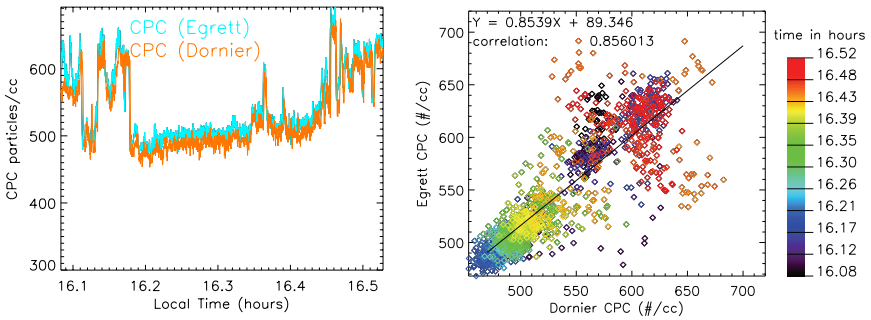

Fig. 4. Egrett and Dornier CPC data on the intercomparison flight. Left: time line for the two CPCs. Right: scatter plot.

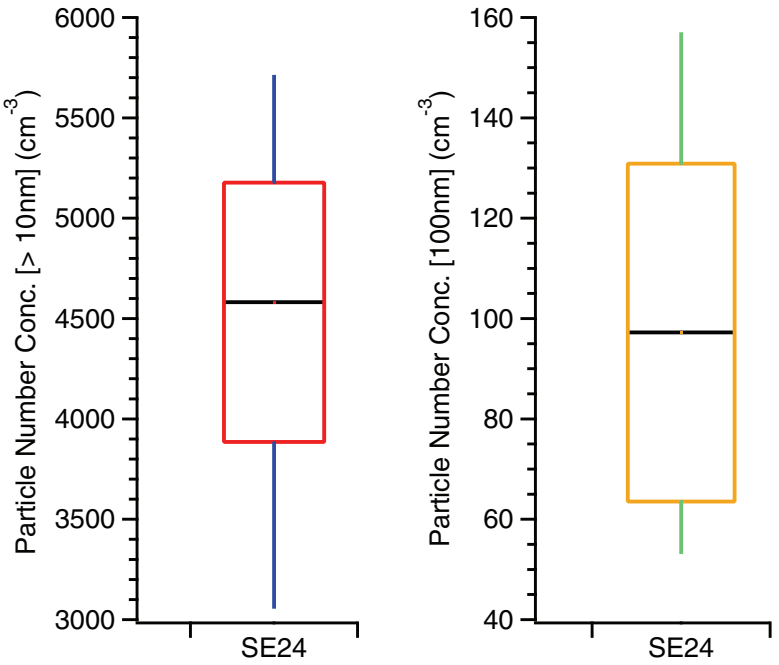

Fig. 5. Box-whisker plots summarising aerosol concentrations measured by the two Egrett CPCs above 10 km, averaged over 50 s (~ 5 km) data bins, on flight SE24 on 3 February 2006. The centre line is the median, the boxes denote the 75 percentile and the whiskers the 90 and 10 percentiles. Left panel: CPC1 (> 10 nm); right panel: CPC2 (with diffusion disks).

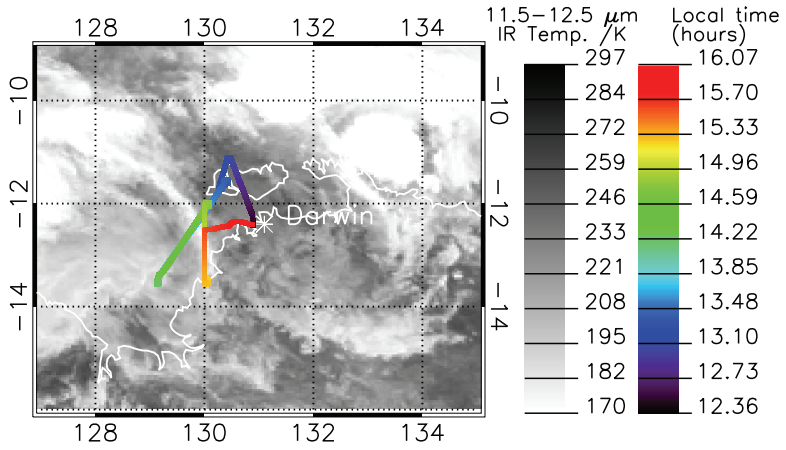

Fig. 6. Egrett flight path, colour-coded with the local time, superimposed on an MTSAT channel 2 image (11.5–12.5 µm). The MTSAT image, over the Darwin area, was taken at approximately 13:20 LT.

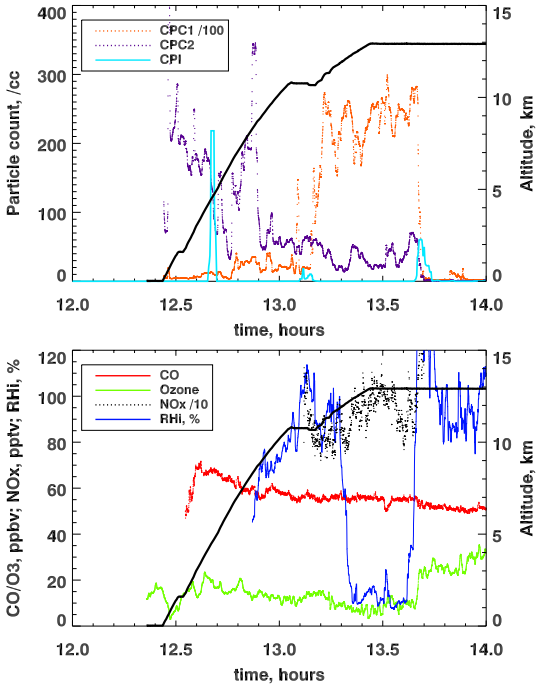

Fig. 7. First 1.5 h of flight, over the Tiwi Islands. The thick black line denotes aircraft altitude (km), while the other lines are as shown in the key. Note the marked increase in aerosol concentration as the aircraft exits cloud at 13.17 h and decrease as it enters cloud again at 13.65 h. The sharp drop in humidity at 13.32 h was observed independently by the three hygrometers but does not correspond to any feature in the other three tracers (CO, O_3, NO_x). Between 13 and 14 h the potential temperature measured by the aircraft was 350–355 K.

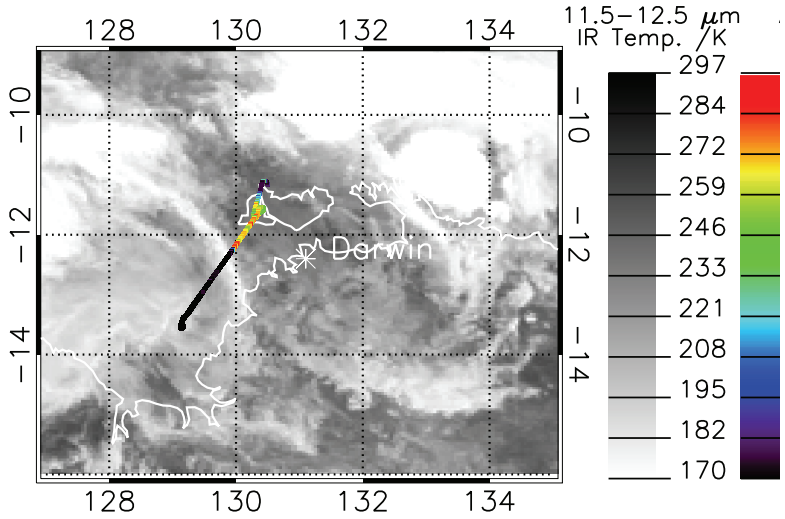

Fig. 8. Infrared satellite image as in Fig. 6, overlaid with the flight section of Fig. 7. The flight track is colour coded with aerosol concentration for the 10–100 nm size range.

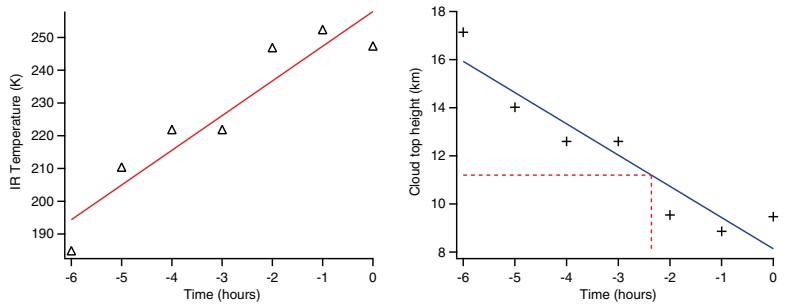

Fig. 9. Variation along a trajectory taken from the above section (Fig. 8). The left-hand plot shows the infrared temperature with time along the trajectory. The right-hand plot shows cloud top height derived from the temperature; the red dashed line marks the Egrett altitude and the time when this intersected the cloud top height, so that this trajectory was taken as exiting cloud 2.3 h prior to the aircraft observation.

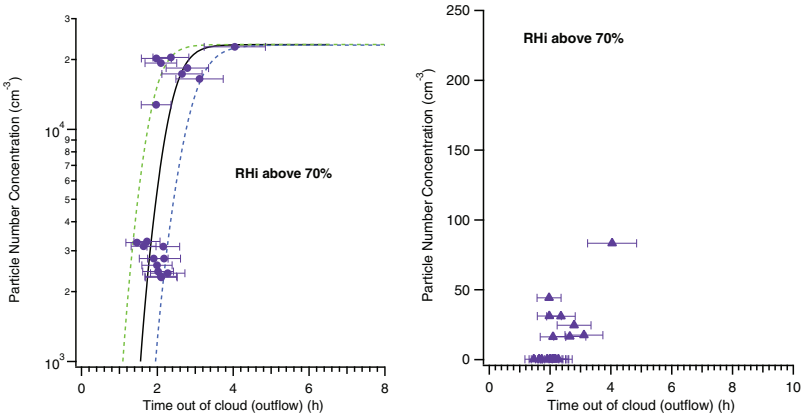

Fig. 10. Triangular symbols: particle number concentration (STP) for the Aitken mode (10–100 nm, left-hand plot), and the accumulation mode (100–1000 nm, right-hand plot) aerosol, against the time since the trajectory exited cloud. Markers indicate median particle number concentrations for the 5 km flight sections, and are fitted with the solid sigmoid curve. Dashed lines are the same but with cloud temperatures modified by ± 5 K; these indicate the sensitivity of the method to the assumption that the infrared radiance is a measure of cloud top height. Note that the left-hand plot has a log-scale *y*-axis and the right hand has a linear scale.

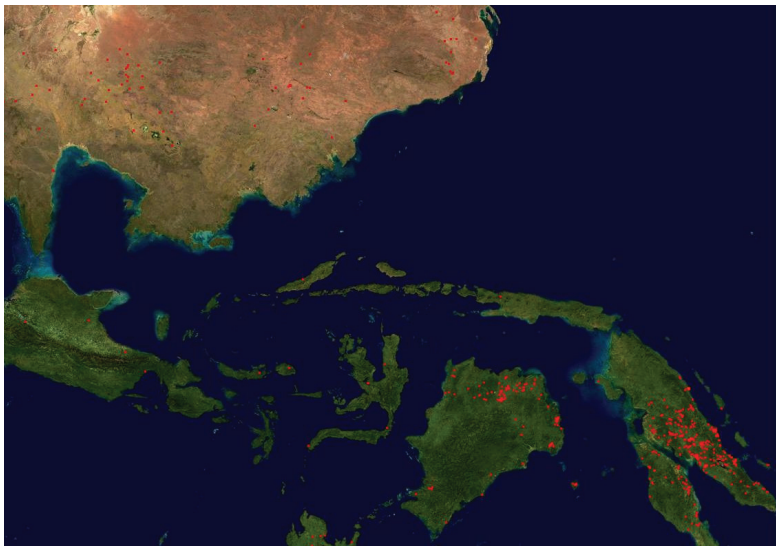

Fig. 11. MODIS fire map for the period 22–30 January 2006, courtesy of http://rapidfire.sci.gsfc.nasa.gov/firemaps/.

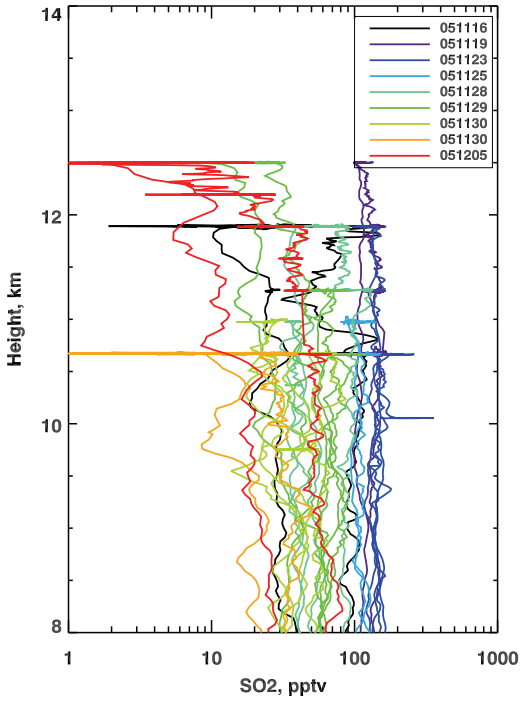

Fig. 12. Compilation of all SO_2 data obtained in the altitude range 8–12.5 km, on the 9 FALCON missions conducted between 16 November and 5 December 2005 as part of the SCOUT-O3 campaign. At 10–12 km altitude the mean and median SO_2 mixing ratios are both around 100 pptv, with 75 % and 90 % percentiles around 130 pptv and 160 pptv. Note how the SO_2 concentration decreases as the campaign progresses (cool colours at the start, warm at the end).

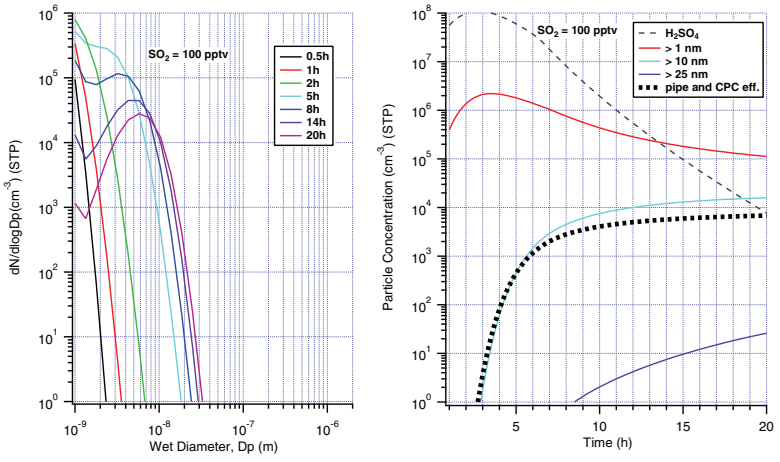

Fig. 13. Left: aerosol size distribution as a function of wet diameter, *Dp*. The background SO_2 concentration was set at 100 pptv and the acid production was semi-sinusoidally varied to replicate daylight hours. Concentration is adjusted to STP units. Right: concentrations calculated numerically as a function of time for molecular sulphuric acid (H_2SO_4), total aerosol number (above 0.5 nm), and aerosol numbers with diameters over 9 nm and 24 nm. Bold dotted line shows expected counts on the unmodified CPC, using the efficiency curve of Eq. (1) and the pipework transmission function.